arXiv:1003.2923v1 [hep-ex] 15 Mar 2010

DESY–10–034
March 2010

Inclusive-jet cross sections in NC DIS at HERA and a comparison of the k_T, anti-k_T and SIScone jet algorithms

ZEUS Collaboration

Abstract

For the first time, differential inclusive-jet cross sections have been measured in neutral current deep inelastic ep scattering using the anti-k_T and SIScone algorithms. The measurements were made for boson virtualities $Q^2 > 125$ GeV^2 with the ZEUS detector at HERA using an integrated luminosity of 82 pb^{-1} and the jets were identified in the Breit frame. The performance and suitability of the jet algorithms for their use in hadron-like reactions were investigated by comparing the measurements to those performed with the k_T algorithm. Next-to-leading-order QCD calculations give a good description of the measurements. Measurements of the ratios of cross sections using different jet algorithms are also presented; the measured ratios are well described by calculations including up to $\mathcal{O}(\alpha_s^3)$ terms. Values of $\alpha_s(M_Z)$ were extracted from the data; the results are compatible with and have similar precision to the value extracted from the k_T analysis.

The ZEUS Collaboration

H. Abramowicz[44,ad], I. Abt[34], L. Adamczyk[13], M. Adamus[53], R. Aggarwal[7], S. Antonelli[4], P. Antonioli[3], A. Antonov[32], M. Arneodo[49], V. Aushev[26,y], Y. Aushev[26,y], O. Bachynska[15], A. Bamberger[19], A.N. Barakbaev[25], G. Barbagli[17], G. Bari[3], F. Barreiro[29], D. Bartsch[5], M. Basile[4], O. Behnke[15], J. Behr[15], U. Behrens[15], L. Bellagamba[3], A. Bertolin[38], S. Bhadra[56], M. Bindi[4], C. Blohm[15], T. Bołd[13], E.G. Boos[25], M. Borodin[26], K. Borras[15], D. Boscherini[3], D. Bot[15], S.K. Boutle[51], I. Brock[5], E. Brownson[55], R. Brugnera[39], N. Brümmer[36], A. Bruni[3], G. Bruni[3], B. Brzozowska[52], P.J. Bussey[20], J.M. Butterworth[51], B. Bylsma[36], A. Caldwell[34], M. Capua[8], R. Carlin[39], C.D. Catterall[56], S. Chekanov[1], J. Chwastowski[12,f], J. Ciborowski[52,ai], R. Ciesielski[15,h], L. Cifarelli[4], F. Cindolo[3], A. Contin[4], A.M. Cooper-Sarkar[37], N. Coppola[15,i], M. Corradi[3], F. Corriveau[30], M. Costa[48], G. D'Agostini[42], F. Dal Corso[38], J. de Favereau[28], J. del Peso[29], R.K. Dementiev[33], S. De Pasquale[4,b], M. Derrick[1], R.C.E. Devenish[37], D. Dobur[19], B.A. Dolgoshein[32], A.T. Doyle[20], V. Drugakov[16], L.S. Durkin[36], S. Dusini[38], Y. Eisenberg[54], P.F. Ermolov [33,†], A. Eskreys[12], S. Fang[15], S. Fazio[8], J. Ferrando[37], M.I. Ferrero[48], J. Figiel[12], M. Forrest[20], B. Foster[37], S. Fourletov[50,ah], G. Gach[13], A. Galas[12], E. Gallo[17], A. Garfagnini[39], A. Geiser[15], I. Gialas[21,u], L.K. Gladilin[33], D. Gladkov[32], C. Glasman[29], O. Gogota[26], Yu.A. Golubkov[33], P. Göttlicher[15,j], I. Grabowska-Bołd[13], J. Grebenyuk[15], I. Gregor[15], G. Grigorescu[35], G. Grzelak[52], C. Gwenlan[37,aa], T. Haas[15], W. Hain[15], R. Hamatsu[47], J.C. Hart[43], H. Hartmann[5], G. Hartner[56], E. Hilger[5], D. Hochman[54], U. Holm[22], R. Hori[46], K. Horton[37,ab], A. Hüttmann[15], G. Iacobucci[3], Z.A. Ibrahim[10], Y. Iga[41], R. Ingbir[44], M. Ishitsuka[45], H.-P. Jakob[5], F. Januschek[15], M. Jimenez[29], T.W. Jones[51], M. Jüngst[5], I. Kadenko[26], B. Kahle[15], B. Kamaluddin [10,†], S. Kananov[44], T. Kanno[45], U. Karshon[54], F. Karstens[19], I.I. Katkov[15,k], M. Kaur[7], P. Kaur[7,d], A. Keramidas[35], L.A. Khein[33], J.Y. Kim[9], D. Kisielewska[13], S. Kitamura[47,ae], R. Klanner[22], U. Klein[15,l], E. Koffeman[35], D. Kollar[34], P. Kooijman[35], Ie. Korol[26], I.A. Korzhavina[33], A. Kotański[14,g], U. Kötz[15], H. Kowalski[15], P. Kulinski[52], O. Kuprash[26], M. Kuze[45], V.A. Kuzmin[33], A. Lee[36], B.B. Levchenko[33,z], A. Levy[44], V. Libov[15], S. Limentani[39], T.Y. Ling[36], M. Lisovyi[15], E. Lobodzinska[15], W. Lohmann[16], B. Löhr[15], E. Lohrmann[22], J.H. Loizides[51], K.R. Long[23], A. Longhin[38], D. Lontkovskyi[26], O.Yu. Lukina[33], P. Łużniak[52,aj], J. Maeda[45], S. Magill[1], I. Makarenko[26], J. Malka[52,aj], R. Mankel[15,m], A. Margotti[3], G. Marini[42], J.F. Martin[50], A. Mastroberardino[8], T. Matsumoto[24,v], M.C.K. Mattingly[2], I.-A. Melzer-Pellmann[15], S. Miglioranzi[15,n], F. Mohamad Idris[10], V. Monaco[48], A. Montanari[15], J.D. Morris[6,c], B. Musgrave[1], K. Nagano[24], T. Namsoo[15,o], R. Nania[3], D. Nicholass[1,a], A. Nigro[42], Y. Ning[11], U. Noor[56], D. Notz[15], R.J. Nowak[52], A.E. Nuncio-Quiroz[5], B.Y. Oh[40], N. Okazaki[46], K. Oliver[37], K. Olkiewicz[12], Yu. Onishchuk[26], O. Ota[47,af], K. Papageorgiu[21], A. Parenti[15], E. Paul[5], J.M. Pawlak[52], B. Pawlik[12], P. G. Pelfer[18], A. Pellegrino[35], W. Perlanski[52,aj], H. Perrey[22], K. Piotrzkowski[28],

P. Plucinski[53,ak], N.S. Pokrovskiy[25], A. Polini[3], A.S. Proskuryakov[33], M. Przybycień[13], A. Raval[15], D.D. Reeder[55], B. Reisert[34], Z. Ren[11], J. Repond[1], Y.D. Ri[47,ag], A. Robertson[37], P. Roloff[15], E. Ron[29], I. Rubinsky[15], M. Ruspa[49], R. Sacchi[48], A. Salii[26], U. Samson[5], G. Sartorelli[4], A.A. Savin[55], D.H. Saxon[20], M. Schioppa[8], S. Schlenstedt[16], P. Schleper[22], W.B. Schmidke[34], U. Schneekloth[15], V. Schönberg[5], T. Schörner-Sadenius[22], J. Schwartz[30], F. Sciulli[11], L.M. Shcheglova[33], R. Shehzadi[5], S. Shimizu[46,n], I. Singh[7,d], I.O. Skillicorn[20], W. Słomiński[14], W.H. Smith[55], V. Sola[48], A. Solano[48], D. Son[27], V. Sosnovtsev[32], A. Spiridonov[15,p], H. Stadie[22], L. Stanco[38], A. Stern[44], T.P. Stewart[50], A. Stifutkin[32], P. Stopa[12], S. Suchkov[32], G. Susinno[8], L. Suszycki[13], J. Sztuk[22], D. Szuba[15,q], J. Szuba[15,r], A.D. Tapper[23], E. Tassi[8,e], J. Terrón[29], T. Theedt[15], H. Tiecke[35], K. Tokushuku[24,w], O. Tomalak[26], J. Tomaszewska[15,s], T. Tsurugai[31], M. Turcato[22], T. Tymieniecka[53,al], C. Uribe-Estrada[29], M. Vázquez[35,n], A. Verbytskyi[15], V. Viazlo[26], N.N. Vlasov[19,t], O. Volynets[26], R. Walczak[37], W.A.T. Wan Abdullah[10], J.J. Whitmore[40,ac], J. Whyte[56], L. Wiggers[35], M. Wing[51], M. Wlasenko[5], G. Wolf[15], H. Wolfe[55], K. Wrona[15], A.G. Yagües-Molina[15], S. Yamada[24], Y. Yamazaki[24,x], R. Yoshida[1], C. Youngman[15], A.F. Żarnecki[52], L. Zawiejski[12], O. Zenaiev[26], W. Zeuner[15,n], B.O. Zhautykov[25], N. Zhmak[26,y], C. Zhou[30], A. Zichichi[4], M. Zolko[26], D.S. Zotkin[33], Z. Zulkapli[10]

[1] *Argonne National Laboratory, Argonne, Illinois 60439-4815, USA* [A]
[2] *Andrews University, Berrien Springs, Michigan 49104-0380, USA*
[3] *INFN Bologna, Bologna, Italy* [B]
[4] *University and INFN Bologna, Bologna, Italy* [B]
[5] *Physikalisches Institut der Universität Bonn, Bonn, Germany* [C]
[6] *H.H. Wills Physics Laboratory, University of Bristol, Bristol, United Kingdom* [D]
[7] *Panjab University, Department of Physics, Chandigarh, India*
[8] *Calabria University, Physics Department and INFN, Cosenza, Italy* [B]
[9] *Institute for Universe and Elementary Particles, Chonnam National University, Kwangju, South Korea*
[10] *Jabatan Fizik, Universiti Malaya, 50603 Kuala Lumpur, Malaysia* [E]
[11] *Nevis Laboratories, Columbia University, Irvington on Hudson, New York 10027, USA* [F]
[12] *The Henryk Niewodniczanski Institute of Nuclear Physics, Polish Academy of Sciences, Cracow, Poland* [G]
[13] *Faculty of Physics and Applied Computer Science, AGH-University of Science and Technology, Cracow, Poland* [H]
[14] *Department of Physics, Jagellonian University, Cracow, Poland*
[15] *Deutsches Elektronen-Synchrotron DESY, Hamburg, Germany*
[16] *Deutsches Elektronen-Synchrotron DESY, Zeuthen, Germany*
[17] *INFN Florence, Florence, Italy* [B]
[18] *University and INFN Florence, Florence, Italy* [B]
[19] *Fakultät für Physik der Universität Freiburg i.Br., Freiburg i.Br., Germany* [C]
[20] *Department of Physics and Astronomy, University of Glasgow, Glasgow, United Kingdom* [D]
[21] *Department of Engineering in Management and Finance, Univ. of the Aegean, Chios, Greece*
[22] *Hamburg University, Institute of Exp. Physics, Hamburg, Germany* [C]
[23] *Imperial College London, High Energy Nuclear Physics Group, London, United Kingdom* [D]
[24] *Institute of Particle and Nuclear Studies, KEK, Tsukuba, Japan* [I]
[25] *Institute of Physics and Technology of Ministry of Education and Science of Kazakhstan, Almaty, Kazakhstan*
[26] *Institute for Nuclear Research, National Academy of Sciences, and Kiev National University, Kiev, Ukraine*
[27] *Kyungpook National University, Center for High Energy Physics, Daegu, South Korea* [J]

[28] *Institut de Physique Nucléaire, Université Catholique de Louvain, Louvain-la-Neuve, Belgium* [K]
[29] *Departamento de Física Teórica, Universidad Autónoma de Madrid, Madrid, Spain* [L]
[30] *Department of Physics, McGill University, Montréal, Québec, Canada H3A 2T8* [M]
[31] *Meiji Gakuin University, Faculty of General Education, Yokohama, Japan* [I]
[32] *Moscow Engineering Physics Institute, Moscow, Russia* [N]
[33] *Moscow State University, Institute of Nuclear Physics, Moscow, Russia* [O]
[34] *Max-Planck-Institut für Physik, München, Germany*
[35] *NIKHEF and University of Amsterdam, Amsterdam, Netherlands* [P]
[36] *Physics Department, Ohio State University, Columbus, Ohio 43210, USA* [A]
[37] *Department of Physics, University of Oxford, Oxford, United Kingdom* [D]
[38] *INFN Padova, Padova, Italy* [B]
[39] *Dipartimento di Fisica dell' Università and INFN, Padova, Italy* [B]
[40] *Department of Physics, Pennsylvania State University, University Park, Pennsylvania 16802, USA* [F]
[41] *Polytechnic University, Sagamihara, Japan* [I]
[42] *Dipartimento di Fisica, Università 'La Sapienza' and INFN, Rome, Italy* [B]
[43] *Rutherford Appleton Laboratory, Chilton, Didcot, Oxon, United Kingdom* [D]
[44] *Raymond and Beverly Sackler Faculty of Exact Sciences, School of Physics, Tel Aviv University, Tel Aviv, Israel* [Q]
[45] *Department of Physics, Tokyo Institute of Technology, Tokyo, Japan* [I]
[46] *Department of Physics, University of Tokyo, Tokyo, Japan* [I]
[47] *Tokyo Metropolitan University, Department of Physics, Tokyo, Japan* [I]
[48] *Università di Torino and INFN, Torino, Italy* [B]
[49] *Università del Piemonte Orientale, Novara, and INFN, Torino, Italy* [B]
[50] *Department of Physics, University of Toronto, Toronto, Ontario, Canada M5S 1A7* [M]
[51] *Physics and Astronomy Department, University College London, London, United Kingdom* [D]
[52] *Warsaw University, Institute of Experimental Physics, Warsaw, Poland*
[53] *Institute for Nuclear Studies, Warsaw, Poland*
[54] *Department of Particle Physics, Weizmann Institute, Rehovot, Israel* [R]
[55] *Department of Physics, University of Wisconsin, Madison, Wisconsin 53706, USA* [A]
[56] *Department of Physics, York University, Ontario, Canada M3J 1P3* [M]

[A] supported by the US Department of Energy
[B] supported by the Italian National Institute for Nuclear Physics (INFN)
[C] supported by the German Federal Ministry for Education and Research (BMBF), under contract Nos. 05 HZ6PDA, 05 HZ6GUA, 05 HZ6VFA and 05 HZ4KHA
[D] supported by the Science and Technology Facilities Council, UK
[E] supported by an FRGS grant from the Malaysian government
[F] supported by the US National Science Foundation. Any opinion, findings and conclusions or recommendations expressed in this material are those of the authors and do not necessarily reflect the views of the National Science Foundation.
[G] supported by the Polish Ministry of Science and Higher Education as a scientific project No. DPN/N188/DESY/2009
[H] supported by the Polish Ministry of Science and Higher Education as a scientific project (2009-2010)
[I] supported by the Japanese Ministry of Education, Culture, Sports, Science and Technology (MEXT) and its grants for Scientific Research
[J] supported by the Korean Ministry of Education and Korea Science and Engineering Foundation
[K] supported by FNRS and its associated funds (IISN and FRIA) and by an Inter-University Attraction Poles Programme subsidised by the Belgian Federal Science Policy Office
[L] supported by the Spanish Ministry of Education and Science through funds provided by CICYT
[M] supported by the Natural Sciences and Engineering Research Council of Canada (NSERC)
[N] partially supported by the German Federal Ministry for Education and Research (BMBF)
[O] supported by RF Presidential grant N 1456.2008.2 for the leading scientific schools and by the Russian Ministry of Education and Science through its grant for Scientific Research on High Energy Physics
[P] supported by the Netherlands Foundation for Research on Matter (FOM)
[Q] supported by the Israel Science Foundation
[R] supported in part by the MINERVA Gesellschaft für Forschung GmbH, the Israel Science Foundation (grant No. 293/02-11.2) and the US-Israel Binational Science Foundation

[a] also affiliated with University College London, United Kingdom
[b] now at University of Salerno, Italy
[c] now at Queen Mary University of London, United Kingdom
[d] also working at Max Planck Institute, Munich, Germany
[e] also Senior Alexander von Humboldt Research Fellow at Hamburg University, Institute of Experimental Physics, Hamburg, Germany
[f] also at Cracow University of Technology, Faculty of Physics, Mathemathics and Applied Computer Science, Poland
[g] supported by the research grant No. 1 P03B 04529 (2005-2008)
[h] now at Rockefeller University, New York, NY 10065, USA
[i] now at DESY group FS-CFEL-1
[j] now at DESY group FEB, Hamburg, Germany
[k] also at Moscow State University, Russia
[l] now at University of Liverpool, United Kingdom
[m] on leave of absence at CERN, Geneva, Switzerland
[n] now at CERN, Geneva, Switzerland
[o] now at Goldman Sachs, London, UK
[p] also at Institute of Theoretical and Experimental Physics, Moscow, Russia
[q] also at INP, Cracow, Poland
[r] also at FPACS, AGH-UST, Cracow, Poland
[s] partially supported by Warsaw University, Poland
[t] partially supported by Moscow State University, Russia
[u] also affiliated with DESY, Germany
[v] now at Japan Synchrotron Radiation Research Institute (JASRI), Hyogo, Japan
[w] also at University of Tokyo, Japan
[x] now at Kobe University, Japan
[y] supported by DESY, Germany
[z] partially supported by Russian Foundation for Basic Research grant No. 05-02-39028-NSFC-a
[†] deceased
[aa] STFC Advanced Fellow
[ab] nee Korcsak-Gorzo
[ac] This material was based on work supported by the National Science Foundation, while working at the Foundation.
[ad] also at Max Planck Institute, Munich, Germany, Alexander von Humboldt Research Award
[ae] now at Nihon Institute of Medical Science, Japan
[af] now at SunMelx Co. Ltd., Tokyo, Japan
[ag] now at Osaka University, Osaka, Japan

[ah] now at University of Bonn, Germany
[ai] also at Łódź University, Poland
[aj] member of Łódź University, Poland
[ak] now at Lund University, Lund, Sweden
[al] also at University of Podlasie, Siedlce, Poland

1 Introduction

Jet production at high transverse energies in neutral-current (NC) deep inelastic ep scattering (DIS) at HERA provides unique tests of perturbative QCD (pQCD) in a cleaner hadron-like enviroment than that encountered in hadron-hadron collisions. In NC DIS, the jet search is performed in the Breit frame [1] in which, at leading order (LO) in the strong coupling constant, α_s, the boson-gluon-fusion ($V^*g \to q\bar{q}$, with $V = \gamma, Z^0$) and QCD-Compton ($V^*q \to qg$) processes give rise to two hard jets with opposite transverse momenta.

In previous publications, the observables used to test pQCD included inclusive-jet [2–9], dijet [4, 6, 9–11] and multijet [9, 12–14] cross sections and the internal structure of jets [15–18] defined using the k_T cluster algorithm [19] in the longitudinally invariant inclusive mode [20]. These studies demonstrated that this jet algorithm results in the smallest uncertainties in the reconstruction of jets in ep collisions. The k_T algorithm is well suited for ep collisions and yields infrared- and collinear-safe cross sections at any order of pQCD. However, it might not be best suited to reconstruct jets in hadron-hadron collisions, such as those at the LHC. In order to optimise the reconstruction of jet observables in such environments, new algorithms were recently developed, like the anti-k_T [21], a recombination-type jet algorithm, and the "Seedless Infrared-Safe" cone (SIScone) [22] algorithms. The measurements of jet cross sections in NC DIS using these algorithms provide additional tests of QCD and also a test of their performance with data in a well understood hadron-induced reaction.

This letter presents measurements of differential inclusive-jet cross sections as a function of the jet transverse energy in the Breit frame, $E_{T,\mathrm{B}}^{\mathrm{jet}}$, and the virtuality of the exchanged boson, Q^2, based on the anti-k_T and SIScone jet algorithms. Differential inclusive-jet cross sections as functions of $E_{T,\mathrm{B}}^{\mathrm{jet}}$ in different regions of Q^2 are also presented. The analysis is based on the same data sample which was used in recent publications [4, 5] to make cross-section measurements with the k_T jet algorithm. The results are compared with next-to-leading-order (NLO) QCD calculations using recent parameterisations of the parton distribution functions (PDFs) of the proton [23–25] and with previous measurements based on the k_T algorithm. Furthermore, measurements of the ratios of inclusive-jet cross sections using different jet algorithms are presented and compared to pQCD calculations including up to $\mathcal{O}(\alpha_s^3)$ terms. In addition, new determinations of $\alpha_s(M_Z)$ were obtained so as to quantify the performance of the anti-k_T and SIScone algorithms in comparison with that of the k_T analysis.

2 Jet algorithms

The study of jet production in hadronic reactions has been well established as a testing ground of pQCD. Such tests rely on a trustworthy reconstruction of the topology of the final-state partons. This is best done by using jet algorithms with analogous implementation in experiment and theory. On the experimental side, the results of the application of a jet algorithm should not depend significantly on the presence of soft particles or particles which undergo strong decays. On the theoretical side, they should be infrared and collinear safe, so that order-by-order pQCD calculations can be performed. A close correspondence between the jets and the final-state partons, so that hadronisation corrections are small, and suppression of beam-remnant jet contributions, when necessary, are also required.

There are two different methods to reconstruct jets from the final-state particles: cluster- and cone-type algorithms. Cluster algorithms, such as JADE [26] or k_T, are based on successive recombinations of particles. They are usually applied in e^+e^- experiments, where the initial state is governed by QED and the final-state hadrons arise uniquely from the short-distance interaction so that all hadrons observed should be associated with the hard process and thus clustered. Cone algorithms, such as the iterative cone algorithm [27], are based on a maximisation of the energy density within a cone of fixed size and are usually applied in hadron collisions, where the initial state consists of coloured partons. The initial parton carries only a fraction of the momentum of the parent hadron, and the spectator partons lead to the presence of remnant jets and the underlying event, which leads to the production of soft hadrons not correlated with the hard interaction. Thus, not all final-state particles would be associated to jets.

In NC DIS, jets are usually defined using the transverse-energy flow in the pseudorapidity ($\eta_{\rm B}$)−azimuth ($\phi_{\rm B}$) plane of the Breit frame. The procedure to reconstruct jets with the k_T algorithm from an initial list of objects (e.g. final-state partons, final-state hadrons or energy deposits in the calorimeter) is described below in some detail. In the following discussion, $E^i_{T,{\rm B}}$ denotes the transverse energy, $\eta^i_{\rm B}$ the pseudorapidity and $\phi^i_{\rm B}$ the azimuthal angle of object i in the Breit frame. For each pair of objects, the quantity

$$d_{ij} = \min((E^i_{T,{\rm B}})^2, (E^j_{T,{\rm B}})^2) \cdot [(\eta^i_{\rm B} - \eta^j_{\rm B})^2 + (\phi^i_{\rm B} - \phi^j_{\rm B})^2]/R^2 \qquad (1)$$

is calculated. For each individual object, the distance to the beam, $d_i = (E^i_{T,{\rm B}})^2$, is also calculated. If, of all the values $\{d_{ij}, d_i\}$, d_{kl} is the smallest, then objects k and l are combined into a single new object. If, however, d_k is the smallest, then object k is considered a jet and removed from the sample. The procedure is repeated until all objects are assigned to jets.

The k_T algorithm is infrared and collinear safe to all orders in pQCD. As a result of the distance between objects defined in Eq. (1), the jets thus obtained have irregular shapes [28], in contrast to jets defined using a cone algorithm. From an experimental point of view, it may be desirable for jets to have a well-defined shape, e.g. to calibrate the jet-energy scale or to estimate the underlying-event contribution. On the other hand, cone algorithms produce jets that have an approximate circular shape in the pseudorapidity-azimuth plane. However, most implementations of cone algorithms rely on "seeds" to start the search for stable cones, which results in unsafe infrared and collinear behaviour beyond a given order in pQCD.

Recently, new jet algorithms have been proposed which produce jets with an approximate circular shape but maintain the infrared and collinear safety to all orders in pQCD. Two approaches have been followed. The SIScone jet algorithm has been developed to overcome the seed problem. A new recombination-type algorithm, the anti-k_T, has been devised which, after a modification of the distance as defined in Eq. (1), yields circular jets.

The SIScone algorithm consists of two steps. First, for a given set of initial objects, all stable cones are identified; cones are classified as stable by the coincidence of the cone axis with that defined by the total momentum of the objects contained in the given cone of radius R in the $\eta_{\rm B} - \phi_{\rm B}$ plane of the Breit frame. In this procedure, no seed is used. Stable cones are then discarded if their transverse momentum is below a given threshold, $p_{t,\min}$. For each selected stable cone, the scalar sum of the transverse momentum of the objects associated to it, $\tilde{p}_t$, is defined. Second, overlapping cones are identified and subsequently split or merged according to the following procedure. Two cones are merged if the scalar sum of the transverse momentum of the objects shared by the two cones exceeds a certain fraction f of the lowest-$\tilde{p}_t$ cone; otherwise, two different cones are considered and the common objects are assigned to the nearest cone. This jet algorithm is infrared and collinear safe to all orders in pQCD.

The k_T and anti-k_T algorithms are identical except for a modified distance measure,

$$d_{ij} = \min((E^i_{T,\rm B})^{-2}, (E^j_{T,\rm B})^{-2}) \cdot [(\eta^i_{\rm B} - \eta^j_{\rm B})^2 + (\phi^i_{\rm B} - \phi^j_{\rm B})^2]/R^2, \tag{2}$$

and the distance to the beam, which is defined as $d_i = (E^i_{T,\rm B})^{-2}$. This procedure preserves the infrared and collinear safety of the k_T algorithm and, in addition, gives rise to circular jets.

For the measurements presented in this letter, the parameter R was set to unity and the jet variables were defined according to the Snowmass convention [29]. In the application of the SIScone algorithm, the fraction f was set to 0.75 and the transverse momentum threshold $p_{t,\min}$ was set to zero.

3 Experimental set-up

A detailed description of the ZEUS detector can be found elsewhere [30, 31]. A brief outline of the components that are most relevant for this analysis is given below.

Charged particles were tracked in the central tracking detector (CTD) [32], which operated in a magnetic field of 1.43 T provided by a thin superconducting solenoid. The CTD consisted of 72 cylindrical drift-chamber layers, organised in nine superlayers covering the polar-angle[1] region $15^\circ < \theta < 164^\circ$. The transverse-momentum resolution for full-length tracks can be parameterised as $\sigma(p_T)/p_T = 0.0058 p_T \oplus 0.0065 \oplus 0.0014/p_T$, with p_T in GeV. The tracking system was used to measure the interaction vertex with a typical resolution along (transverse to) the beam direction of 0.4 (0.1) cm and to cross-check the energy scale of the calorimeter.

The high-resolution uranium–scintillator calorimeter (CAL) [33] covered 99.7% of the total solid angle and consisted of three parts: the forward (FCAL), the barrel (BCAL) and the rear (RCAL) calorimeters. Each part was subdivided transversely into towers and longitudinally into one electromagnetic section and either one (in RCAL) or two (in BCAL and FCAL) hadronic sections. The smallest subdivision of the calorimeter was called a cell. Under test-beam conditions, the CAL single-particle relative energy resolutions were $\sigma(E)/E = 0.18/\sqrt{E}$ for electrons and $\sigma(E)/E = 0.35/\sqrt{E}$ for hadrons, with E in GeV.

The luminosity was measured from the rate of the bremsstrahlung process $ep \to e\gamma p$. The resulting small-angle energetic photons were measured by the luminosity monitor [34], a lead–scintillator calorimeter placed in the HERA tunnel at $Z = -107$ m.

4 Data selection

The data were collected during the running period 1998–2000, when HERA operated with protons of energy $E_p = 920$ GeV and electrons[2] of energy $E_e = 27.5$ GeV, and correspond to an integrated luminosity of 81.7 ± 1.8 pb^{-1}, of which 16.7 pb^{-1} (65.0 pb^{-1}) was for e^-p (e^+p) collisions.

Neutral current DIS events were selected using the same criteria as reported in recent publications [4, 5]. The main steps are briefly listed below.

[1] The ZEUS coordinate system is a right-handed Cartesian system, with the Z axis pointing in the proton beam direction, referred to as the "forward direction", and the X axis pointing towards the centre of HERA. The coordinate origin is at the nominal interaction point.

[2] Here and in the following, the term "electron" denotes generically both the electron (e^-) and the positron (e^+).

The scattered-electron candidate was identified from the pattern of energy deposits in the CAL [35]. The energy (E'_e) and polar angle of the electron candidate were determined from the CAL measurements. The Q^2 variable was reconstructed using the double-angle method [36]. The angle γ_h, which corresponds to the angle of the scattered quark in the quark-parton model, was reconstructed using the hadronic final state [36].

The main requirements imposed on the data sample were: an electron candidate with $E'_e > 10$ GeV; a vertex position along the beam axis in the range $|Z| < 34$ cm; $38 < (E - P_Z) < 65$ GeV, where E is the total energy as measured by the CAL, $E = \sum_i E_i$, and P_Z is the Z component of the vector $\boldsymbol{P} = \sum_i E_i \hat{\boldsymbol{r}}_i$; in both cases the sum runs over all CAL cells, E_i is the energy of the CAL cell i and $\hat{\boldsymbol{r}}_i$ is a unit vector along the line joining the reconstructed vertex and the geometric centre of the cell i; $Q^2 > 125$ GeV^2; and $|\cos\gamma_h| < 0.65$. In this selected sample, contamination from non-ep interactions and other physics processes was negligible.

The anti-k_T and SIScone algorithms[3] were both used to reconstruct jets in the hadronic final state both in data and in Monte Carlo (MC) simulated events (see Section 5). In the data, the algorithms were applied to the energy deposits measured in the CAL cells after excluding those associated with the scattered-electron candidate. After reconstructing the jet variables in the Breit frame, the massless four-momenta were boosted into the laboratory frame, where the transverse energy ($E^{\rm jet}_{T,\rm LAB}$) and the pseudorapidity ($\eta^{\rm jet}_{\rm LAB}$) of each jet were calculated. Energy corrections [2, 15, 38] were then applied to the jets in the laboratory frame, separately for the anti-k_T and SIScone jet samples. In addition, events were removed from the samples if any of the jets was in the backward region of the detector ($\eta^{\rm jet}_{\rm LAB} < -2$) and jets were not included in the final samples if $E^{\rm jet}_{T,\rm LAB} < 2.5$ GeV.

Only events with at least one jet in the pseudorapidity range $-2 < \eta^{\rm jet}_{\rm B} < 1.5$ were kept for further analysis. The final data samples with at least one jet satisfying $E^{\rm jet}_{T,\rm B} > 8$ GeV contained 18847 events (12575 one-jet, 6126 two-jet, 145 three-jet and one four-jet) in the anti-k_T sample and 19486 events (13081 one-jet, 6252 two-jet, 152 three-jet and one four-jet) in the SIScone sample.

5 Monte Carlo simulation

Samples of events were generated to determine the response of the detector to jets of hadrons and to compute the correction factors necessary to obtain the hadron-level jet cross sections. The hadron level is defined by those hadrons with lifetime $\tau \geq 10$ ps.

[3] The implementations of the anti-k_T and SIScone algorithms in the FASTJET package [37], version 2.4.1, were used.

The generated events were passed through the GEANT 3.13-based [39] ZEUS detector- and trigger-simulation programs [31]. They were reconstructed and analysed by the same program chain as the data.

Neutral current DIS events including electroweak radiative effects were simulated using the HERACLES 4.6.1 [40] program with the DJANGOH 1.1 [41] interface to the QCD programs. The QCD cascade was simulated using the colour-dipole model (CDM) [42] including the LO QCD diagrams as implemented in ARIADNE 4.08 [43] and, alternatively, with the MEPS model of LEPTO 6.5 [44]. The CTEQ5D [45] parameterisations of the proton PDFs were used for these simulations. Fragmentation into hadrons was performed using the Lund string model [46] as implemented in JETSET [47, 48].

The jet search was performed on the simulated events using the energy measured in the CAL cells in the same way as for the data. The same jet algorithms were also applied to the final-state particles (hadron level) and to the partons available after the parton shower (parton level). Additional MC samples were used to correct the measured cross sections for QED radiative effects and the running of $\alpha_{\rm em}$.

6 Acceptance corrections and experimental uncertainties

To measure the cross sections, the $E^{\rm jet}_{T,{\rm B}}$ and Q^2 distributions in the data were corrected for detector effects using bin-by-bin correction factors determined with the MC samples. These correction factors took into account the efficiency of the selection criteria and the purity and efficiency of the jet reconstruction. For this approach to be valid, the uncorrected distributions of the data must be well described by the MC simulations at the detector level. This condition was satisfied by both the ARIADNE and LEPTO-MEPS MC samples. The average between the acceptance-correction values obtained with ARIADNE and LEPTO-MEPS was used to correct the data to the hadron level. The deviations in the results obtained by using either ARIADNE or LEPTO-MEPS to correct the data from their average were taken to represent systematic uncertainties of the effect of the QCD-cascade model in the corrections (see below). The acceptance-correction factors differed from unity by typically less than 10%.

The following sources of systematic uncertainty were considered for the measured cross sections:

- the uncertainty in the absolute energy scale of the jets was estimated to be $\pm 1\%$ for $E^{\rm jet}_{T,{\rm LAB}} > 10$ GeV and $\pm 3\%$ for lower $E^{\rm jet}_{T,{\rm LAB}}$ values [38, 49, 50]. The resulting uncertainty on the cross sections was about $\pm 5\%$;

- the differences in the results obtained by using either ARIADNE or LEPTO-MEPS to correct the data for detector effects were taken to represent systematic uncertainties. The resulting uncertainty on the cross sections was typically below $\pm 3\%$;
- the uncertainty due to the selection cuts was estimated by varying the values of the cuts within the resolution of each variable; the effect on the cross sections was typically below $\pm 3\%$;
- the uncertainty on the reconstruction of the boost to the Breit frame was estimated by using the direction of the track associated with the scattered electron instead of that derived from its impact position in the CAL. The effect on the cross sections was typically below $\pm 1\%$;
- the uncertainty in the absolute energy scale of the electron candidate was estimated to be $\pm 1\%$ [51]. The resulting uncertainty on the cross sections was below $\pm 1\%$;
- the uncertainty in the cross sections due to that in the simulation of the trigger was negligible.

The systematic uncertainties were similar for both jet algorithms. Those not associated with the absolute energy scale of the jets were added in quadrature to the statistical uncertainties and are shown in the figures as error bars. The uncertainty due to the absolute energy scale of the jets is shown separately as a shaded band due to the large bin-to-bin correlation. In addition, there was an overall normalisation uncertainty of 2.2% from the luminosity determination, which is not included in the figures.

7 QCD calculations and theoretical uncertainties

Next-to-leading-order ($\mathcal{O}(\alpha_s^2)$) QCD calculations were compared to the measured inclusive-jet cross sections. The calculations were obtained using the program DISENT [52], in the $\overline{\text{MS}}$ renormalisation and factorisation schemes using a generalised version [52] of the subtraction method [53]. The number of flavours was set to five and the renormalisation (μ_R) and factorisation (μ_F) scales were chosen to be $\mu_R = E_{T,\text{B}}^{\text{jet}}$ and $\mu_F = Q$, respectively. The strong coupling constant was calculated at two loops with $\Lambda_{\overline{\text{MS}}}^{(5)} = 226$ MeV, corresponding to $\alpha_s(M_Z) = 0.118$. The calculations were performed using the ZEUS-S [23] parameterisations of the proton PDFs[4]. In DISENT, the value of α_{em} was fixed to 1/137. The anti-k_T and SIScone algorithms were also applied to the partons in the events generated by DISENT in order to compute the jet cross-section predictions.

[4] The LHAPDF package [54], version 5.7.1, was used.

Measurements are also presented of the ratio of inclusive-jet cross sections based on different jet algorithms. Although the calculations for inclusive-jet cross sections can be made at present only up to $\mathcal{O}(\alpha_s^2)$ (see Fig. 1), the differences[5] of cross sections using different jet algorithms can be predicted up to $\mathcal{O}(\alpha_s^3)$ using the program NLOJET++ [55]. The same parameter settings as defined above were used for the NLOJET++ predictions. The predicted ratio $(d\sigma_{\text{anti}-k_T}/dX)/(d\sigma_{k_T}/dX)$, where $X = Q^2$ or $E_{T,\text{B}}^{\text{jet}}$, was calculated as

$$\frac{d\sigma_{\text{anti}-k_T}/dX}{d\sigma_{k_T}/dX} = 1 + \frac{d\sigma_{\text{anti}-k_T}/dX - d\sigma_{k_T}/dX}{d\sigma_{k_T}/dX} \simeq 1 + \frac{C \cdot \alpha_s^3}{A \cdot \alpha_s + B \cdot \alpha_s^2}, \tag{3}$$

since differences between the anti-k_T and k_T algorithms appear first for final states with four partons and were evaluated using the tree-level $eq \to eqggg$, $eq \to eqgq\bar{q}$, $eg \to eq\bar{q}q\bar{q}$ and $eg \to eggq\bar{q}$ subprocesses (see Fig. 1). The predicted ratio $(d\sigma_{\text{SIScone}}/dX)/(d\sigma_{k_T}/dX)$ was calculated as

$$\frac{d\sigma_{\text{SIScone}}/dX}{d\sigma_{k_T}/dX} = 1 + \frac{d\sigma_{\text{SIScone}}/dX - d\sigma_{k_T}/dX}{d\sigma_{k_T}/dX} \simeq 1 + \frac{D \cdot \alpha_s^2 + E \cdot \alpha_s^3}{A \cdot \alpha_s + B \cdot \alpha_s^2}, \tag{4}$$

since differences between the SIScone and k_T algorithms appear first for final states with three partons and were evaluated using the tree-level three-parton and four-parton subprocesses and the one-loop three-parton configurations (see Fig. 1). Equation (4) also applies to the predicted ratio $(d\sigma_{\text{anti}-k_T}/dX)/(d\sigma_{\text{SIScone}}/dX)$.

Since the measurements refer to jets of hadrons, whereas the NLO QCD calculations refer to jets of partons, the predictions were corrected to the hadron level using the MC models. The multiplicative correction factor (C_{had}) was defined as the ratio of the cross section for jets of hadrons over that for jets of partons, estimated by using the MC programs described in Section 5. The mean of the ratios obtained with ARIADNE and LEPTO-MEPS was taken as the value of C_{had}. The value of C_{had} for the inclusive-jet cross sections differs from unity by less than 5% [5], 6% and 11% for the k_T, anti-k_T and SIScone jet algorithms, respectively, in the region $Q^2 \geq 500$ GeV^2.

Neither DISENT nor NLOJET++ include the contribution from Z^0 exchange; MC simulated events with and without Z^0 exchange were used to include this effect in the pQCD predictions. In the following, pQCD calculations refer to the fully corrected predictions.

Several sources of uncertainty in the theoretical predictions for the inclusive-jet cross sections were considered:

- the uncertainty on the NLO QCD calculations due to terms beyond NLO, estimated by varying μ_R between $E_{T,\text{B}}^{\text{jet}}/2$ and $2E_{T,\text{B}}^{\text{jet}}$, was below ± 7 (± 10)% at low Q^2 and low

[5] The differences of cross sections were evaluated on an event-by-event basis.

$E^{\rm jet}_{T,\rm B}$ and decreased to less than ± 5 $(\pm 7)\%$ for $Q^2 > 250$ GeV^2 for the k_T [5] and anti-k_T (SIScone) algorithms;

- the uncertainty on the NLO QCD calculations due to those on the proton PDFs was estimated by repeating the calculations using 22 additional sets from the ZEUS-S analysis, which takes into account the statistical and correlated systematic experimental uncertainties of each data set used in the determination of the proton PDFs. The resulting uncertainty in the cross sections for all three jet algorithms was below $\pm 3\%$, except in the high-$E^{\rm jet}_{T,\rm B}$ region where it reached $\pm 4\%$;
- the uncertainty on the NLO QCD calculations due to that on $\alpha_s(M_Z)$ was estimated by repeating the calculations using two additional sets of proton PDFs, for which different values of $\alpha_s(M_Z)$ were assumed in the fits. The difference between the calculations using these various sets was scaled by a factor to reflect the uncertainty on the current world average of α_s [56]. The resulting uncertainty in the cross sections was below $\pm 2\%$ for all three jet algorithms;
- the uncertainty from the modelling of the QCD cascade was assumed to be half the difference between the hadronisation corrections obtained using the Ariadne and Lepto-MEPS models. The resulting uncertainty on the cross sections was less than $\pm 1.4\%$ [5], $\pm 1.7\%$ and $\pm 2.3\%$ for the k_T, anti-k_T and SIScone algorithms, respectively;
- the uncertainty of the calculations due to the choice of μ_F was estimated by repeating the calculations with $\mu_F = Q/2$ and $2Q$. The effect was negligible.

The total theoretical uncertainty was obtained by adding in quadrature the individual uncertainties listed above. As a function of Q^2, the total theoretical uncertainty varies in the range $3-7\%$ $(3-10\%)$ for the anti-k_T (SIScone) algorithm; as a function of $E^{\rm jet}_{T,\rm B}$, the range of variation is $5-6\%$ $(6-8\%)$ for the anti-k_T (SIScone) algorithm.

It is concluded that the NLO QCD predictions for the inclusive-jet cross sections are of similar precision for the k_T and anti-k_T algorithms and somewhat less precise for the SIScone. A more detailed comparison of the theoretical uncertainties is presented in Section 8.

8 Results

8.1 Inclusive-jet differential cross sections with different jet algorithms

The inclusive-jet differential cross sections were measured in the kinematic region $Q^2 > 125$ GeV^2 and $|\cos\gamma_h| < 0.65$. The jets were reconstructed using either the anti-k_T or

the SIScone jet algorithms and the cross sections refer to jets with $E_{T,\mathrm{B}}^{\mathrm{jet}} > 8$ GeV and $-2 < \eta_{\mathrm{B}}^{\mathrm{jet}} < 1.5$. These cross sections were corrected for detector and QED radiative effects and the running of α_{em}.

The measurements of the inclusive-jet differential cross sections as functions of $E_{T,\mathrm{B}}^{\mathrm{jet}}$ and Q^2 are presented in Fig. 2 and Tables 1 and 2 for the anti-k_T and SIScone jet algorithms. For comparison, the measurements of inclusive-jet cross sections with the k_T algorithm [5] are also shown. In Fig. 2, each data point is plotted at the abscissa at which the NLO QCD differential cross section was equal to its bin-averaged value. The measured $d\sigma/dE_{T,\mathrm{B}}^{\mathrm{jet}}$ ($d\sigma/dQ^2$) exhibits a steep fall-off over three (five) orders of magnitude for the jet algorithms considered in the $E_{T,\mathrm{B}}^{\mathrm{jet}}$ (Q^2) measured range. The measurements using the three jet algorithms have a very similar shape and normalisation.

The NLO QCD predictions with $\mu_R = E_{T,\mathrm{B}}^{\mathrm{jet}}$ are compared to the measurements in Fig. 2. The hadronisation-correction factors and their uncertainties are also shown. The ratios of the measured differential cross sections to the NLO QCD calculations are shown in Figs. 3a and 3b separately for each jet algorithm. The measured differential cross sections are well reproduced by the calculations, with similar precision in all cases. To study the scale dependence, NLO QCD calculations using $\mu_R = Q$ were also compared to the data (not shown); they also provide a good description of the data.

To compare in more detail the results of the different algorithms, the ratios of the measured cross-sections anti-k_T/k_T, SIScone/k_T and anti-k_T/SIScone were investigated (see Figs. 3c and 3d). In the ratios, the statistical correlations among the event samples as well as those among the jets in the same event were taken into account in the estimation of the statistical uncertainties. These ratios show that the cross sections with the three jet algorithms are similar: the ratios as functions of Q^2 differ from unity by less than 3.2%; as functions of $E_{T,\mathrm{B}}^{\mathrm{jet}}$, they differ by less than 3.6% except at high $E_{T,\mathrm{B}}^{\mathrm{jet}}$, where the difference is 10%. The pQCD predictions including up to $\mathcal{O}(\alpha_s^3)$ terms for the ratios of cross sections are also shown in Figs. 3c and 3d. In the estimation of the total theoretical uncertainty of the predicted ratio, all the theoretical contributions were assumed to be correlated except that due to terms beyond $\mathcal{O}(\alpha_s^3)$ and that from the modelling of the QCD cascade. The measured ratios are well described by the calculations including up to $\mathcal{O}(\alpha_s^3)$ terms within the small experimental and theoretical uncertainties, which are dominated by the uncertainty on the modelling of the QCD cascade.

Figure 4 shows the contributions to the theoretical uncertainty of the inclusive-jet cross sections from terms beyond NLO, from the uncertainty in the PDFs, from that on the value of $\alpha_s(M_Z)$ and from that on the modelling of the QCD cascade, separately for the anti-k_T and SIScone algorithms. The uncertainty coming from the terms beyond NLO is dominant at low $E_{T,\mathrm{B}}^{\mathrm{jet}}$ and low Q^2 in all cases and somewhat higher for the predictions based on SIScone than those for the anti-k_T and k_T [5] algorithms. At high $E_{T,\mathrm{B}}^{\mathrm{jet}}$, the PDF

uncertainty is dominant in the case of the anti-k_T algorithm and of the same order as that arising from terms beyond NLO for the SIScone algorithm. At high Q^2, the uncertainty due to terms beyond NLO is of the same order for both algorithms and remains dominant. The uncertainty on the modelling of the QCD cascade is somewhat higher for the SIScone algorithm than for anti-k_T, but significantly smaller than that from terms beyond NLO. The total theoretical uncertainty for the predictions using $\mu_R = Q$ is slightly larger than that using $\mu_R = E^{\rm jet}_{T,\rm B}$.

The inclusive-jet cross sections for different regions of Q^2 as a function of $E^{\rm jet}_{T,\rm B}$ are presented in Fig. 5 and Tables 3 and 4 for both algorithms. The measured cross sections exhibit a steep fall-off within the $E^{\rm jet}_{T,\rm B}$ range considered. As Q^2 increases, the $E^{\rm jet}_{T,\rm B}$ dependence of the cross section becomes less steep. The measurements have a similar shape and normalisation for both jet algorithms and are similar to the results obtained with the k_T algorithm [4]. The NLO QCD predictions are compared to the measurements in Fig. 5. The data are well described by the predictions. Figure 6 shows the ratios of the measured differential cross sections to the NLO QCD calculations. The uncertainty of the NLO QCD calculations is also shown: the uncertainties from the anti-k_T predictions are of a similar size as those encountered for the k_T algorithm [4], and those for SIScone are somewhat larger at low $E^{\rm jet}_{T,\rm B}$ and low Q^2.

In summary, it is concluded that the data for the k_T, anti-k_T and SIScone jet algorithms are well described by the NLO QCD calculations with similar experimental and theoretical precision. Furthermore, the measured ratios are well described by the predictions including up to $\mathcal{O}(\alpha_s^3)$ terms, demonstrating the ability of the pQCD calculations with up to four partons in the final state to account adequately for the differences between the jet algorithms.

8.2 Determination of $\alpha_s(M_Z)$

The measured differential cross-sections $d\sigma/dQ^2$ for $Q^2 > 500$ GeV^2 were used to determine values of $\alpha_s(M_Z)$ using the method presented previously [2]. The NLO QCD calculations were performed using the program DISENT with five sets of ZEUS-S proton PDFs which were determined from global fits assuming different values of $\alpha_s(M_Z)$, namely $\alpha_s(M_Z) = 0.115,\ 0.117,\ 0.119,\ 0.121$ and 0.123. The value of $\alpha_s(M_Z)$ used in each calculation was that associated with the corresponding set of PDFs. The $\alpha_s(M_Z)$ dependence of the predicted cross sections in each bin i of Q^2 was parameterised according to

$$\left[d\sigma/dQ^2(\alpha_s(M_Z))\right]_i = C_1^i \alpha_s(M_Z) + C_2^i \alpha_s^2(M_Z),$$

where C_1^i and C_2^i were determined from a χ^2 fit to the NLO QCD calculations. The value

of $\alpha_s(M_Z)$ was determined by a χ^2 fit to the measured $d\sigma/dQ^2$ values.

The uncertainties on the extracted values of $\alpha_s(M_Z)$ due to the experimental systematic uncertainties were evaluated by repeating the analysis for each systematic check presented in Section 6. The overall normalisation uncertainty from the luminosity determination was also considered. The largest contribution to the experimental uncertainty comes from the jet energy scale and amounts to $\pm 1.9\%$ on $\alpha_s(M_Z)$ for both algorithms ($\pm 2\%$ for k_T [5]). The theoretical uncertainties were evaluated as described in Section 7. The largest contribution was the theoretical uncertainty arising from terms beyond NLO, which was estimated by using the method proposed by Jones et al. [57], and amounted to $\pm 1.5\%$ for both algorithms[6] ($\pm 1.5\%$ for k_T [5]). The uncertainty due to the proton PDFs was ± 0.7 (± 0.8)% for the anti-k_T (SIScone) algorithm ($\pm 0.7\%$ for k_T [5]). The uncertainty arising from the hadronisation effects amounted to ± 0.9 (± 1.2)% for the anti-k_T (SIScone) algorithm ($\pm 0.8\%$ for k_T [5]). Thus, the performance of the three jet algorithms is very similar.

As a cross-check, $\alpha_s(M_Z)$ was determined by using NLO QCD calculations based on the CTEQ6.1 [24] (MSTW2008 [25]) sets of proton PDFs: the values obtained are consistent within ± 1.2 (± 1.0)% with those based on ZEUS-S. The uncertainty arising from the proton PDFs was estimated to be ± 1.5 (± 0.7, ± 0.4)% using the results of the CTEQ6.1 (MSTW2008nlo90cl, MSTW2008nlo68cl) analysis.

The values of $\alpha_s(M_Z)$ obtained from the measured $d\sigma/dQ^2$ for $Q^2 > 500$ GeV^2 are

$$\begin{aligned}
\alpha_s(M_Z)|_{\text{anti}-k_T} &= 0.1188 \pm 0.0014\ (\text{stat.})\ ^{+0.0033}_{-0.0032}\ (\text{exp.})\ ^{+0.0022}_{-0.0022}\ (\text{th.}) \text{ and} \\
\alpha_s(M_Z)|_{\text{SIScone}} &= 0.1186 \pm 0.0013\ (\text{stat.})\ ^{+0.0034}_{-0.0032}\ (\text{exp.})\ ^{+0.0025}_{-0.0025}\ (\text{th.}).
\end{aligned}$$

These values of $\alpha_s(M_Z)$ are consistent with that obtained using the k_T algorithm [5],

$$\alpha_s(M_Z)|_{\text{k}_\text{T}} = 0.1207 \pm 0.0014\ (\text{stat.})\ ^{+0.0035}_{-0.0033}\ (\text{exp.})\ ^{+0.0022}_{-0.0023}\ (\text{th.}),$$

with the current world average of 0.1189 ± 0.0010 [56], with the results obtained in $p\bar{p}$ collisions [58] as well as with the HERA average of 0.1186 ± 0.0051 [59]. It should be noted that the differences between the central values of $\alpha_s(M_Z)$ obtained using the three jet algorithms are comparable to the uncertainties due to higher-order terms in the calculations. It is observed that the precision in $\alpha_s(M_Z)$ obtained with the k_T, anti-k_T and SIScone jet algorithms is very similar, and comparable to those obtained in e^+e^- interactions [56].

[6] The theoretical uncertainty arising from terms beyond NLO estimated by refitting the data using calculations based on $\mu_R = 2E^{\text{jet}}_{T,\text{B}}$ or $E^{\text{jet}}_{T,\text{B}}/2$ amounts to $^{+2.1}_{-0.0}$ ($^{+3.1}_{-0.7}$)% for the anti-k_T (SIScone) algorithm.

9 Summary and conclusions

For the first time, differential cross sections for inclusive-jet production in neutral current deep inelastic ep scattering were measured using the anti-k_T and SIScone jet algorithms with $R = 1$. The cross sections correspond to a centre-of-mass energy of 318 GeV and refer to jets of hadrons with $E_{T,\mathrm{B}}^{\mathrm{jet}} > 8$ GeV and $-2 < \eta_{\mathrm{B}}^{\mathrm{jet}} < 1.5$ identified in the Breit frame with the anti-k_T or SIScone jet algorithms. The measurements are given in the kinematic region of $Q^2 > 125$ GeV^2 and $|\cos\gamma_h| < 0.65$.

A detailed comparison between the measurements as functions of $E_{T,\mathrm{B}}^{\mathrm{jet}}$ and Q^2 for both algorithms and those from a previous analysis based on the k_T jet reconstruction was performed. The measured cross sections for the three jet algorithms have similar shapes and normalisations.

The NLO QCD calculations of inclusive-jet cross sections and their uncertainties for the different algorithms were also compared: the data are well described by the predictions; the calculations for the anti-k_T algorithm have a similar precision as that of the k_T whereas those for the SIScone are somewhat less precise due to the contribution from terms beyond NLO.

Measurements of the ratios of cross sections using different jet algorithms were also presented and compared to calculations including up to $\mathcal{O}(\alpha_s^3)$ terms. The measured ratios are well reproduced by the predictions, demonstrating the ability of the pQCD calculations including up to four partons in the final state to account adequately for the differences between the jet algorithms.

Values of $\alpha_s(M_Z)$ were extracted from the measured inclusive-jet differential cross sections using each algorithm. QCD fits of the cross-sections $d\sigma/dQ^2$ for $Q^2 > 500$ GeV^2 yield the following values of $\alpha_s(M_Z)$:

$$\begin{aligned}
\alpha_s(M_Z)|_{\mathrm{anti}-k_T} &= 0.1188 \pm 0.0014\ (\mathrm{stat.})\ ^{+0.0033}_{-0.0032}\ (\mathrm{exp.})\ ^{+0.0022}_{-0.0022}\ (\mathrm{th.})\ \text{and} \\
\alpha_s(M_Z)|_{\mathrm{SIScone}} &= 0.1186 \pm 0.0013\ (\mathrm{stat.})\ ^{+0.0034}_{-0.0032}\ (\mathrm{exp.})\ ^{+0.0025}_{-0.0025}\ (\mathrm{th.}).
\end{aligned}$$

These values are consistent with each other and with that obtained from the k_T analysis with a similar precision.

Acknowledgements

We thank the DESY Directorate for their strong support and encouragement. The remarkable achievements of the HERA machine group were essential for the successful completion of this work and are greatly appreciated. We are grateful for the support of the DESY computing and network services. The design, construction and installation of the ZEUS detector have been made possible owing to the ingenuity and effort of many people who are not listed as authors. We would like to thank M. Cacciari, Z. Nagy, G. P. Salam and G. Soyez for useful discussions.

References

[1] R.P. Feynman, *Photon-Hadron Interactions*. Benjamin, New York, (1972); K.H. Streng, T.F. Walsh and P.M. Zerwas, Z. Phys. C 2 (1979) 237.

[2] ZEUS Coll., S. Chekanov et al., Phys. Lett. B 547 (2002) 164.

[3] ZEUS Coll., S. Chekanov et al., Phys. Lett. B 551 (2003) 226.

[4] ZEUS Coll., S. Chekanov et al., Nucl. Phys. B 765 (2007) 1.

[5] ZEUS Coll., S. Chekanov et al., Phys. Lett. B 649 (2007) 12.

[6] H1 Coll., C. Adloff et al., Eur. Phys. J. C 19 (2001) 289.

[7] H1 Coll., C. Adloff et al., Phys. Lett. B 542 (2002) 193.

[8] H1 Coll., A. Aktas et al., Phys. Lett. B 653 (2007) 134.

[9] H1 Coll., F.D. Aaron et al., Eur. Phys. J. C 65 (2010) 363.

[10] ZEUS Coll., J. Breitweg et al., Phys. Lett. B 507 (2001) 70.

[11] ZEUS Coll., S. Chekanov et al., Eur. Phys. J. C 23 (2002) 13.

[12] ZEUS Coll., S. Chekanov et al., Eur. Phys. J. C 44 (2005) 183.

[13] ZEUS Coll., S. Chekanov et al., Preprint DESY-08-100 (hep-ex/0808.3783), DESY, 2008.

[14] H1 Coll., C. Adloff et al., Phys. Lett. B 515 (2001) 17.

[15] ZEUS Coll., S. Chekanov et al., Phys. Lett. B 558 (2003) 41.

[16] ZEUS Coll., S. Chekanov et al., Nucl. Phys. B 700 (2004) 3.

[17] ZEUS Coll., S. Chekanov et al., Eur. Phys. J. C 63 (2009) 527.

[18] H1 Coll., C. Adloff et al., Nucl. Phys. B 545 (1999) 3.

[19] S. Catani et al., Nucl. Phys. B 406 (1993) 187.

[20] S.D. Ellis and D.E. Soper, Phys. Rev. D 48 (1993) 3160.

[21] M. Cacciari, G.P. Salam and G. Soyez, JHEP 04 (2008) 063.

[22] G.P. Salam and G. Soyez, JHEP 05 (2007) 086.

[23] ZEUS Coll., S. Chekanov et al., Phys. Rev. D 67 (2003) 012007.

[24] J. Pumplin et al., JHEP 0207 (2002) 012;
D. Stump et al., JHEP 0310 (2003) 046.

[25] A.D. Martin et al., Eur. Phys. J. C 63 (2009) 189.

[26] JADE Coll., W. Bartel et al., Z. Phys. C 33 (1986) 23;
JADE Coll., S. Bethke et al., Phys. Lett. B 213 (1988) 235.

[27] UA1 Coll., G. Arnison et al., Phys. Lett. B 123 (1983) 115.

[28] M. Cacciari, G.P. Salam and G. Soyez, JHEP 0804 (2008) 005.

[29] J.E. Huth et al., *Research Directions for the Decade. Proc. of Summer Study on High Energy Physics, 1990*, E.L. Berger (ed.), p. 134. World Scientific (1992). Also in preprint FERMILAB-CONF-90-249-E.

[30] ZEUS Coll., M. Derrick et al., Phys. Lett. B 293 (1992) 465.

[31] ZEUS Coll., U. Holm (ed.), *The ZEUS Detector*. Status Report (unpublished), DESY (1993), available on `http://www-zeus.desy.de/bluebook/bluebook.html`.

[32] N. Harnew et al., Nucl. Inst. Meth. A 279 (1989) 290;
B. Foster et al., Nucl. Phys. Proc. Suppl. B 32 (1993) 181;
B. Foster et al., Nucl. Inst. Meth. A 338 (1994) 254.

[33] M. Derrick et al., Nucl. Inst. Meth. A 309 (1991) 77;
A. Andresen et al., Nucl. Inst. Meth. A 309 (1991) 101;
A. Caldwell et al., Nucl. Inst. Meth. A 321 (1992) 356;
A. Bernstein et al., Nucl. Inst. Meth. A 336 (1993) 23.

[34] J. Andruszków et al., Preprint DESY-92-066, DESY, 1992;
ZEUS Coll., M. Derrick et al., Z. Phys. C 63 (1994) 391;
J. Andruszków et al., Acta Phys. Pol. B 32 (2001) 2025.

[35] H. Abramowicz, A. Caldwell and R. Sinkus, Nucl. Inst. Meth. A 365 (1995) 508;
R. Sinkus and T. Voss, Nucl. Inst. Meth. A 391 (1997) 360.

[36] S. Bentvelsen, J. Engelen and P. Kooijman, *Proc. of the Workshop on Physics at HERA*, W. Buchmüller and G. Ingelman (eds.), Vol. 1, p. 23. Hamburg, Germany, DESY (1992);
K.C. Höger, ibid., p. 43.

[37] M. Cacciari and G.P. Salam, Phys. Lett. B 641 (2006) 57.

[38] ZEUS Coll., S. Chekanov et al., Phys. Lett. B 531 (2002) 9.

[39] R. Brun et al., GEANT3, Technical Report CERN-DD/EE/84-1, CERN, 1987.

[40] A. Kwiatkowski, H. Spiesberger and H.-J. Möhring, Comp. Phys. Comm. 69 (1992) 155;
H. Spiesberger, *An Event Generator for ep Interactions at HERA Including Radiative Processes (Version 4.6)*, 1996, available on `http://www.desy.de/~hspiesb/heracles.html`.

[41] K. Charchuła, G.A. Schuler and H. Spiesberger, Comp. Phys. Comm. 81 (1994) 381;
H. Spiesberger, HERACLES *and* DJANGOH*: Event Generation for ep Interactions at HERA Including Radiative Processes*, 1998, available on `http://wwwthep.physik.uni-mainz.de/~hspiesb/djangoh/djangoh.html`.

[42] Y. Azimov et al., Phys. Lett. B 165 (1985) 147;
G. Gustafson, Phys. Lett. B 175 (1986) 453;
G. Gustafson and U. Pettersson, Nucl. Phys. B 306 (1988) 746;
B. Andersson et al., Z. Phys. C 43 (1989) 625.

[43] L. Lönnblad, Comp. Phys. Comm. 71 (1992) 15;
L. Lönnblad, Z. Phys. C 65 (1995) 285.

[44] G. Ingelman, A. Edin and J. Rathsman, Comp. Phys. Comm. 101 (1997) 108.

[45] H.L. Lai et al., Eur. Phys. J. C 12 (2000) 375.

[46] B. Andersson et al., Phys. Rep. 97 (1983) 31.

[47] T. Sjöstrand, Comp. Phys. Comm. 82 (1994) 74;
T. Sjöstrand et al., Comp. Phys. Comm. 135 (2001) 238.

[48] T. Sjöstrand, Comp. Phys. Comm. 39 (1986) 347;
T. Sjöstrand and M. Bengtsson, Comp. Phys. Comm. 43 (1987) 367.

[49] ZEUS Coll., S. Chekanov et al., Eur. Phys. J. C 23 (2002) 615.

[50] M. Wing (on behalf of the ZEUS Coll.), *Proc. of the 10th International Conference on Calorimetry in High Energy Physics*, R. Zhu (ed.), p. 767. Pasadena, USA (2002). Also in preprint hep-ex/0206036.

[51] ZEUS Coll., S. Chekanov et al., Eur. Phys. J. C 21 (2001) 443.

[52] S. Catani and M.H. Seymour, Nucl. Phys. B 485 (1997) 291. Erratum in Nucl. Phys. **B 510** (1998) 503.

[53] R.K. Ellis, D.A. Ross and A.E. Terrano, Nucl. Phys. B 178 (1981) 421.

[54] M.R. Whalley, D. Bourilkov and R.C. Group, Preprint hep-ph/0508110, 2005.

[55] Z. Nagy and Z. Trocsanyi, Phys. Rev. Lett. 87 (2001) 082001.

[56] S. Bethke, J. Phys. G 26 (2000) R27. Updated in S. Bethke, Prog. Part. Nucl. Phys. 58 (2007) 351.

[57] R.W.L. Jones et al., JHEP 0312 (2003) 007.

[58] CDF Coll., T. Affolder et al., Phys. Rev. Lett. 88 (2002) 042001;
DØ Coll., V.M. Abazov et al., Phys. Rev. D 80 (2009) 111107.

[59] C. Glasman, *Proc. of the 13th International Workshop on Deep Inelastic Scattering*, S.R. Dasu and W.H. Smith (eds.), p. 689. Madison, USA (2005). Also in preprint hep-ex/0506035.

$E_{T,\mathrm{B}}^{\mathrm{jet}}$ bin (GeV)	$d\sigma/dE_{T,\mathrm{B}}^{\mathrm{jet}}$ (pb/GeV)	δ_{stat}	δ_{syst}	δ_{ES}	C_{QED}	$C_{\mathrm{had}} \cdot C_{Z^0}$
anti-k_T						
$8-10$	62.84	± 0.69	$^{+1.40}_{-1.49}$	$^{+2.67}_{-2.46}$	0.95	0.93
$10-14$	28.56	± 0.34	$^{+0.39}_{-0.48}$	$^{+1.31}_{-1.25}$	0.97	0.93
$14-18$	10.69	± 0.20	$^{+0.20}_{-0.23}$	$^{+0.57}_{-0.49}$	0.96	0.92
$18-25$	3.186	± 0.082	$^{+0.041}_{-0.040}$	$^{+0.143}_{-0.154}$	0.95	0.92
$25-35$	0.725	± 0.032	$^{+0.014}_{-0.014}$	$^{+0.038}_{-0.034}$	0.94	0.94
$35-100$	0.0300	± 0.0026	$^{+0.0005}_{-0.0006}$	$^{+0.0014}_{-0.0015}$	1.06	0.92
SIScone						
$8-10$	64.08	± 0.69	$^{+1.74}_{-1.82}$	$^{+2.73}_{-2.54}$	0.95	0.87
$10-14$	28.92	± 0.34	$^{+0.42}_{-0.49}$	$^{+1.42}_{-1.29}$	0.96	0.85
$14-18$	10.72	± 0.20	$^{+0.16}_{-0.22}$	$^{+0.55}_{-0.51}$	0.96	0.85
$18-25$	3.211	± 0.081	$^{+0.045}_{-0.043}$	$^{+0.161}_{-0.149}$	0.95	0.85
$25-35$	0.744	± 0.033	$^{+0.017}_{-0.017}$	$^{+0.036}_{-0.039}$	0.93	0.88
$35-100$	0.0332	± 0.0028	$^{+0.0008}_{-0.0008}$	$^{+0.0020}_{-0.0016}$	1.06	0.86

Table 1: *The measured differential cross-sections $d\sigma/dE_{T,\mathrm{B}}^{\mathrm{jet}}$ for inclusive-jet production using different jet algorithms. The statistical, uncorrelated systematic and jet-energy-scale* (ES) *uncertainties are shown separately. The multiplicative corrections applied to the data to correct for QED radiative effects, C_{QED}, and the corrections for hadronisation and Z^0 effects to be applied to the parton-level NLO QCD calculations, $C_{\mathrm{had}} \cdot C_{Z^0}$, are shown in the last two columns.*

Q^2 bin (GeV^2)	$d\sigma/dQ^2$ ($\mathrm{pb/GeV}^2$)	δ_{stat}	δ_{syst}	δ_{ES}	C_{QED}	$C_{\mathrm{had}} \cdot C_{Z^0}$
anti-k_T						
$125 - 250$	1.078	± 0.012	$^{+0.017}_{-0.018}$	$^{+0.067}_{-0.060}$	0.97	0.90
$250 - 500$	0.3589	± 0.0053	$^{+0.0055}_{-0.0084}$	$^{+0.0147}_{-0.0142}$	0.95	0.94
$500 - 1000$	0.1004	± 0.0020	$^{+0.0019}_{-0.0019}$	$^{+0.0030}_{-0.0028}$	0.95	0.94
$1000 - 2000$	0.02406	± 0.00072	$^{+0.00044}_{-0.00033}$	$^{+0.00045}_{-0.00058}$	0.94	0.96
$2000 - 5000$	0.00385	± 0.00017	$^{+0.00015}_{-0.00012}$	$^{+0.00007}_{-0.00007}$	0.94	0.97
$5000 - 100000$	$36.6 \cdot 10^{-6}$	$\pm 3.3 \cdot 10^{-6}$	$^{+2.2}_{-2.6} \cdot 10^{-6}$	$^{+1.0}_{-0.9} \cdot 10^{-6}$	0.98	0.95
SIScone						
$125 - 250$	1.099	± 0.012	$^{+0.020}_{-0.021}$	$^{+0.069}_{-0.063}$	0.97	0.82
$250 - 500$	0.3637	± 0.0053	$^{+0.0062}_{-0.0089}$	$^{+0.0156}_{-0.0143}$	0.95	0.87
$500 - 1000$	0.1011	± 0.0020	$^{+0.0025}_{-0.0024}$	$^{+0.0030}_{-0.0028}$	0.95	0.89
$1000 - 2000$	0.02419	± 0.00071	$^{+0.00048}_{-0.00045}$	$^{+0.00060}_{-0.00057}$	0.94	0.92
$2000 - 5000$	0.00393	± 0.00017	$^{+0.00014}_{-0.00012}$	$^{+0.00007}_{-0.00007}$	0.94	0.93
$5000 - 100000$	$36.8 \cdot 10^{-6}$	$\pm 3.2 \cdot 10^{-6}$	$^{+1.8}_{-2.5} \cdot 10^{-6}$	$^{+1.1}_{-0.6} \cdot 10^{-6}$	0.97	0.92

Table 2: *The measured differential cross-sections $d\sigma/dQ^2$ for inclusive-jet production using different jet algorithms. Other details as in the caption to Table 1.*

$E_{T,\mathrm{B}}^{\mathrm{jet}}$ bin (GeV)	$d\sigma/dE_{T,\mathrm{B}}^{\mathrm{jet}}$ (pb/GeV)	δ_{stat}	δ_{syst}	δ_{ES}	C_{QED}	$C_{\mathrm{had}} \cdot C_{Z^0}$
$125 < Q^2 < 250$ GeV^2						
$8-10$	31.60	± 0.49	$^{+0.90}_{-0.93}$	$^{+1.87}_{-1.56}$	0.95	0.91
$10-14$	12.67	± 0.22	$^{+0.13}_{-0.15}$	$^{+0.80}_{-0.74}$	0.99	0.90
$14-18$	3.56	± 0.11	$^{+0.03}_{-0.05}$	$^{+0.26}_{-0.24}$	0.96	0.88
$18-25$	0.790	± 0.037	$^{+0.013}_{-0.012}$	$^{+0.051}_{-0.047}$	0.95	0.86
$25-100$	0.0165	± 0.0015	$^{+0.0013}_{-0.0013}$	$^{+0.0008}_{-0.0011}$	1.02	0.85
$250 < Q^2 < 500$ GeV^2						
$8-10$	17.90	± 0.38	$^{+0.41}_{-0.50}$	$^{+0.52}_{-0.58}$	0.94	0.94
$10-14$	8.37	± 0.19	$^{+0.18}_{-0.26}$	$^{+0.36}_{-0.32}$	0.96	0.94
$14-18$	3.17	± 0.11	$^{+0.04}_{-0.08}$	$^{+0.18}_{-0.14}$	0.97	0.94
$18-25$	0.882	± 0.042	$^{+0.016}_{-0.015}$	$^{+0.047}_{-0.055}$	0.92	0.89
$25-100$	0.0225	± 0.0020	$^{+0.0006}_{-0.0006}$	$^{+0.0011}_{-0.0011}$	0.94	0.95
$500 < Q^2 < 1000$ GeV^2						
$8-10$	8.36	± 0.26	$^{+0.17}_{-0.18}$	$^{+0.19}_{-0.14}$	0.96	0.95
$10-14$	4.52	± 0.14	$^{+0.14}_{-0.13}$	$^{+0.12}_{-0.13}$	0.94	0.92
$14-18$	2.116	± 0.092	$^{+0.099}_{-0.097}$	$^{+0.069}_{-0.058}$	0.93	0.95
$18-25$	0.682	± 0.039	$^{+0.017}_{-0.016}$	$^{+0.026}_{-0.029}$	0.97	0.95
$25-100$	0.0293	± 0.0025	$^{+0.0014}_{-0.0014}$	$^{+0.0019}_{-0.0016}$	0.94	0.98
$1000 < Q^2 < 2000$ GeV^2						
$8-10$	3.34	± 0.16	$^{+0.10}_{-0.08}$	$^{+0.00}_{-0.10}$	0.93	0.97
$10-14$	1.967	± 0.093	$^{+0.070}_{-0.065}$	$^{+0.025}_{-0.039}$	0.93	0.96
$14-18$	1.099	± 0.068	$^{+0.049}_{-0.048}$	$^{+0.036}_{-0.015}$	0.95	0.94
$18-25$	0.477	± 0.033	$^{+0.024}_{-0.024}$	$^{+0.009}_{-0.011}$	0.94	1.00
$25-100$	0.0237	± 0.0023	$^{+0.0015}_{-0.0015}$	$^{+0.0015}_{-0.0012}$	0.99	0.99
$2000 < Q^2 < 5000$ GeV^2						
$8-10$	1.374	± 0.099	$^{+0.094}_{-0.084}$	$^{+0.034}_{-0.004}$	0.91	0.89
$10-14$	0.797	± 0.059	$^{+0.030}_{-0.022}$	$^{+0.009}_{-0.009}$	0.93	0.96
$14-18$	0.598	± 0.051	$^{+0.032}_{-0.026}$	$^{+0.025}_{-0.012}$	1.01	0.99
$18-25$	0.261	± 0.026	$^{+0.006}_{-0.012}$	$^{+0.005}_{-0.007}$	0.97	1.05
$25-100$	0.0189	± 0.0022	$^{+0.0010}_{-0.0011}$	$^{+0.0007}_{-0.0006}$	0.90	1.02
$5000 < Q^2 < 100000$ GeV^2						
$8-10$	0.301	± 0.051	$^{+0.033}_{-0.037}$	$^{+0.005}_{-0.021}$	0.94	0.89
$10-14$	0.229	± 0.034	$^{+0.007}_{-0.013}$	$^{+0.013}_{-0.005}$	0.96	0.93
$14-18$	0.148	± 0.028	$^{+0.020}_{-0.017}$	$^{+0.000}_{-0.009}$	1.01	0.92
$18-25$	0.081	± 0.016	$^{+0.013}_{-0.014}$	$^{+0.002}_{-0.001}$	0.98	0.99
$25-100$	0.0104	± 0.0020	$^{+0.0007}_{-0.0007}$	$^{+0.0002}_{-0.0001}$	1.00	1.04

Table 3: *The measured differential cross-section $d\sigma/dE_{T,\mathrm{B}}^{\mathrm{jet}}$ for inclusive-jet production in different regions of Q^2 using the anti-k_T jet algorithm. Other details as in the caption to Table 1.*

$E_{T,\mathrm{B}}^{\mathrm{jet}}$ bin (GeV)	$d\sigma/dE_{T,\mathrm{B}}^{\mathrm{jet}}$ (pb/GeV)	δ_{stat}	δ_{syst}	δ_{ES}	C_{QED}	$C_{\mathrm{had}} \cdot C_{Z^0}$
$125 < Q^2 < 250$ GeV^2						
$8-10$	32.36	± 0.49	$^{+0.99}_{-1.02}$	$^{+1.86}_{-1.67}$	0.96	0.84
$10-14$	12.79	± 0.22	$^{+0.17}_{-0.18}$	$^{+0.84}_{-0.78}$	0.98	0.81
$14-18$	3.66	± 0.11	$^{+0.04}_{-0.05}$	$^{+0.26}_{-0.24}$	0.97	0.80
$18-25$	0.792	± 0.037	$^{+0.009}_{-0.008}$	$^{+0.056}_{-0.044}$	0.95	0.79
$25-100$	0.0180	± 0.0015	$^{+0.0013}_{-0.0013}$	$^{+0.0009}_{-0.0012}$	1.00	0.80
$250 < Q^2 < 500$ GeV^2						
$8-10$	18.02	± 0.37	$^{+0.53}_{-0.60}$	$^{+0.59}_{-0.55}$	0.94	0.89
$10-14$	8.55	± 0.19	$^{+0.19}_{-0.24}$	$^{+0.37}_{-0.33}$	0.96	0.87
$14-18$	3.16	± 0.11	$^{+0.04}_{-0.09}$	$^{+0.17}_{-0.15}$	0.97	0.86
$18-25$	0.893	± 0.042	$^{+0.021}_{-0.021}$	$^{+0.055}_{-0.050}$	0.92	0.82
$25-100$	0.0247	± 0.0021	$^{+0.0004}_{-0.0004}$	$^{+0.0012}_{-0.0014}$	0.94	0.87
$500 < Q^2 < 1000$ GeV^2						
$8-10$	8.65	± 0.26	$^{+0.25}_{-0.24}$	$^{+0.14}_{-0.16}$	0.96	0.89
$10-14$	4.49	± 0.14	$^{+0.12}_{-0.11}$	$^{+0.13}_{-0.12}$	0.94	0.88
$14-18$	2.112	± 0.091	$^{+0.074}_{-0.073}$	$^{+0.073}_{-0.067}$	0.94	0.90
$18-25$	0.677	± 0.038	$^{+0.024}_{-0.024}$	$^{+0.031}_{-0.026}$	0.97	0.89
$25-100$	0.0289	± 0.0025	$^{+0.0010}_{-0.0010}$	$^{+0.0016}_{-0.0018}$	0.93	0.89
$1000 < Q^2 < 2000$ GeV^2						
$8-10$	3.30	± 0.16	$^{+0.12}_{-0.11}$	$^{+0.07}_{-0.06}$	0.92	0.94
$10-14$	2.024	± 0.096	$^{+0.080}_{-0.085}$	$^{+0.038}_{-0.036}$	0.95	0.92
$14-18$	1.070	± 0.068	$^{+0.049}_{-0.048}$	$^{+0.024}_{-0.025}$	0.96	0.91
$18-25$	0.478	± 0.033	$^{+0.026}_{-0.025}$	$^{+0.010}_{-0.014}$	0.93	0.93
$25-100$	0.0246	± 0.0024	$^{+0.0018}_{-0.0018}$	$^{+0.0017}_{-0.0012}$	0.98	0.93
$2000 < Q^2 < 5000$ GeV^2						
$8-10$	1.47	± 0.11	$^{+0.07}_{-0.05}$	$^{+0.00}_{-0.04}$	0.94	0.86
$10-14$	0.822	± 0.059	$^{+0.037}_{-0.031}$	$^{+0.020}_{-0.010}$	0.94	0.94
$14-18$	0.563	± 0.049	$^{+0.032}_{-0.034}$	$^{+0.012}_{-0.006}$	0.97	0.92
$18-25$	0.276	± 0.027	$^{+0.010}_{-0.015}$	$^{+0.006}_{-0.012}$	0.98	0.99
$25-100$	0.0186	± 0.0021	$^{+0.0008}_{-0.0008}$	$^{+0.0006}_{-0.0005}$	0.88	0.98
$5000 < Q^2 < 100000$ GeV^2						
$8-10$	0.264	± 0.044	$^{+0.047}_{-0.052}$	$^{+0.014}_{-0.001}$	0.94	0.90
$10-14$	0.248	± 0.036	$^{+0.019}_{-0.024}$	$^{+0.011}_{-0.006}$	0.96	0.90
$14-18$	0.146	± 0.027	$^{+0.011}_{-0.012}$	$^{+0.003}_{-0.002}$	0.99	0.91
$18-25$	0.082	± 0.016	$^{+0.015}_{-0.016}$	$^{+0.002}_{-0.002}$	1.00	0.92
$25-100$	0.0111	± 0.0021	$^{+0.0009}_{-0.0008}$	$^{+0.0004}_{-0.0004}$	1.00	0.99

Table 4: *The measured differential cross-section $d\sigma/dE_{T,\mathrm{B}}^{\mathrm{jet}}$ for inclusive-jet production in different regions of Q^2 using the SIScone jet algorithm. Other details as in the caption to Table 1.*

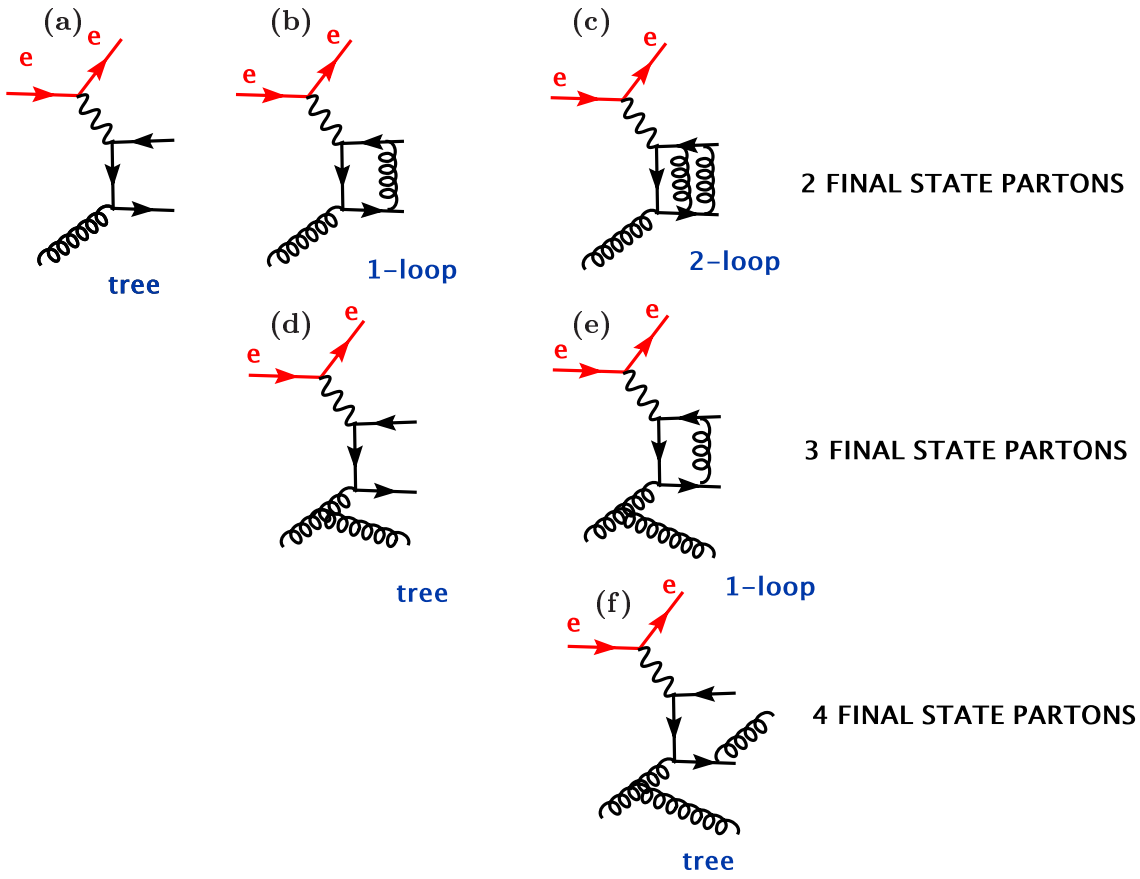

Figure 1: *Examples of Feynman diagrams contributing to inclusive-jet production in the Breit frame up to $\mathcal{O}(\alpha_s^3)$. The calculations of inclusive-jet cross sections up to $\mathcal{O}(\alpha_s^2)$ include the (a) leading-order diagrams and (b) virtual and (d) real corrections. The lowest-order diagrams that contribute to the cross-section difference between the anti-k_T and k_T algorithms are of type (f). The calculations of the cross-section difference between the SIScone and k_T algorithms include diagrams of type (d), (e) and (f).*

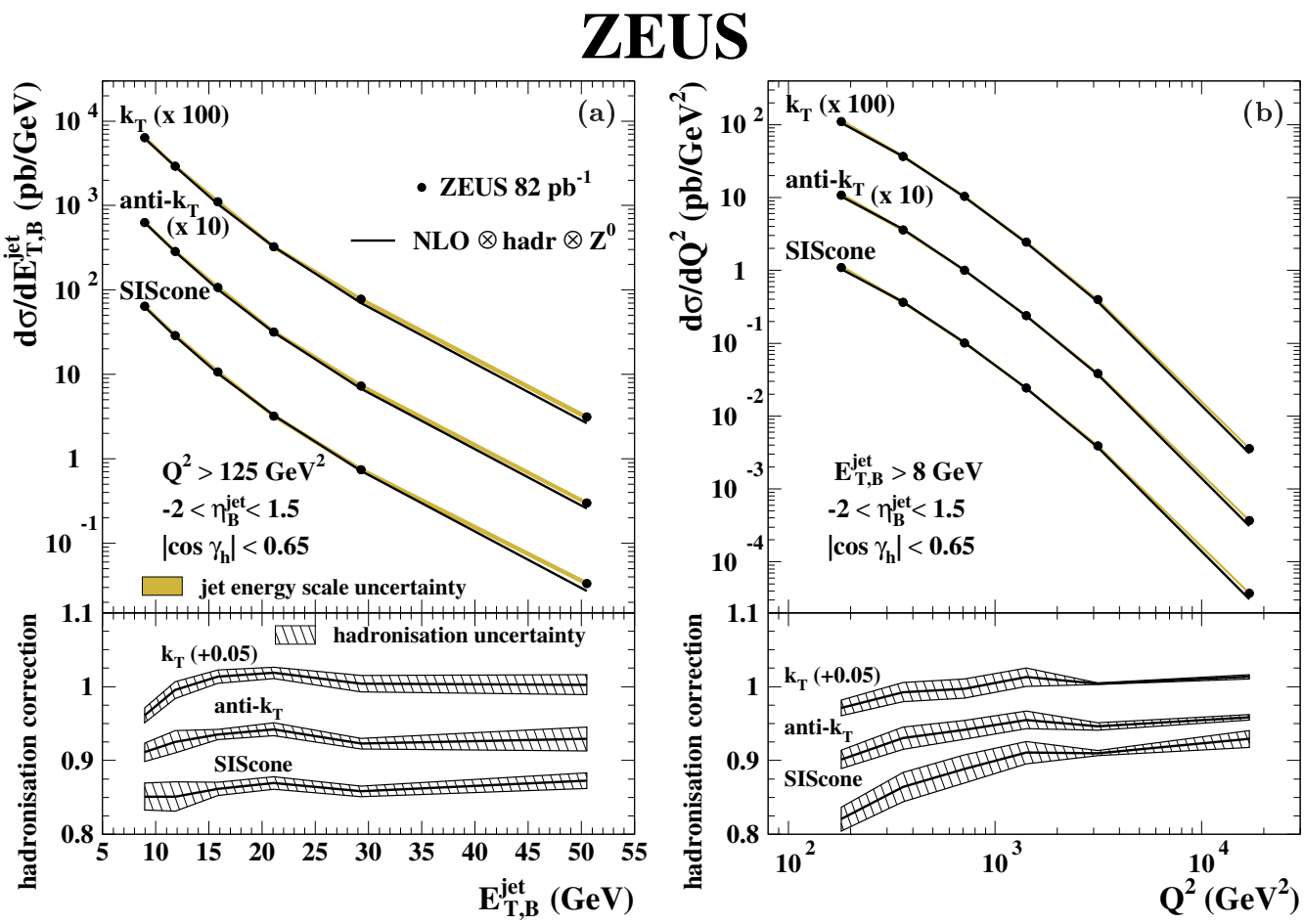

Figure 2: *The measured differential cross-sections (a) $d\sigma/dE^{\rm jet}_{T,\rm B}$ and (b) $d\sigma/dQ^2$ for inclusive-jet production (dots) using different jet algorithms. The NLO QCD calculations with $\mu_R = E^{\rm jet}_{T,\rm B}$ (solid lines) are also shown. The cross sections for the anti-k_T and k_T [5] algorithms were multiplied by the scale factors indicated in brackets to aid visibility. The error bars on the data points are smaller than the marker size and are therefore not visible. The shaded bands display the uncertainty due to the absolute energy scale of the jets. The lower part of the figures shows the hadronisation-correction factor applied to the NLO calculations together with its uncertainty (hatched bands) for each jet algorithm; the hadronisation-correction factor for the k_T algorithm was shifted by the value indicated in brackets to aid visibility.*

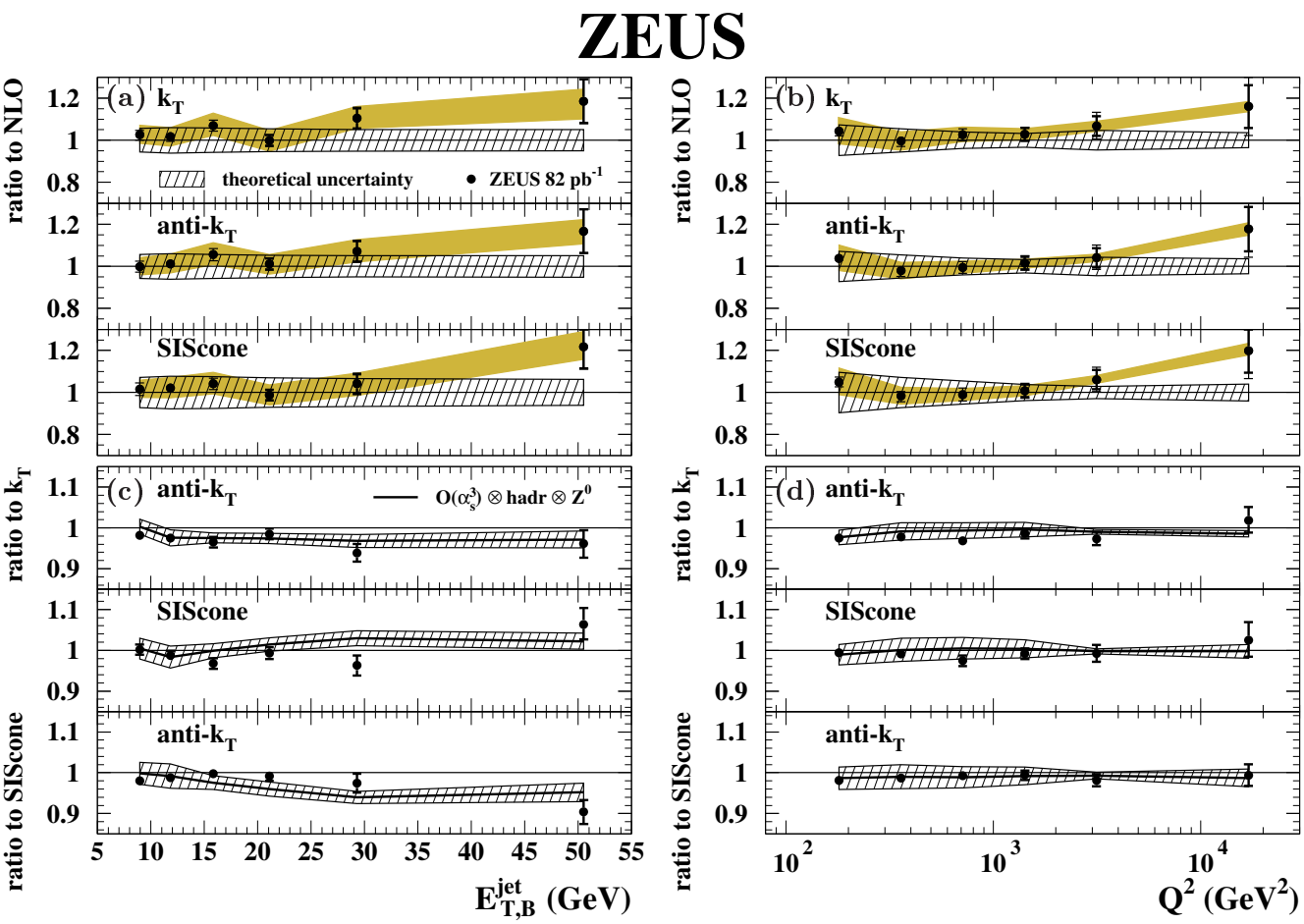

Figure 3: *The ratios between the measured cross-sections (a) $d\sigma/dE^{\rm jet}_{T,\rm B}$ and (b) $d\sigma/dQ^2$ and the NLO QCD calculations (dots). The inner error bars represent the statistical uncertainty. The outer error bars show the statistical and systematic uncertainties, not associated with the uncertainty of the absolute energy scale of the jets, added in quadrature. The hatched bands display the total theoretical uncertainty and the shaded bands display the jet-energy scale uncertainty. The ratios of the measured cross sections (dots) anti-k_T/k_T, SIScone/k_T and anti-k_T/SIScone as functions of (c) $E^{\rm jet}_{T,\rm B}$ and (d) Q^2. In these plots, the outer error bars include also the uncertainty of the absolute energy scale of the jets. The predicted ratios based on calculations which include up to $\mathcal{O}(\alpha_s^3)$ terms are also shown (solid lines). The hatched bands display the theoretical uncertainty on the ratio.*

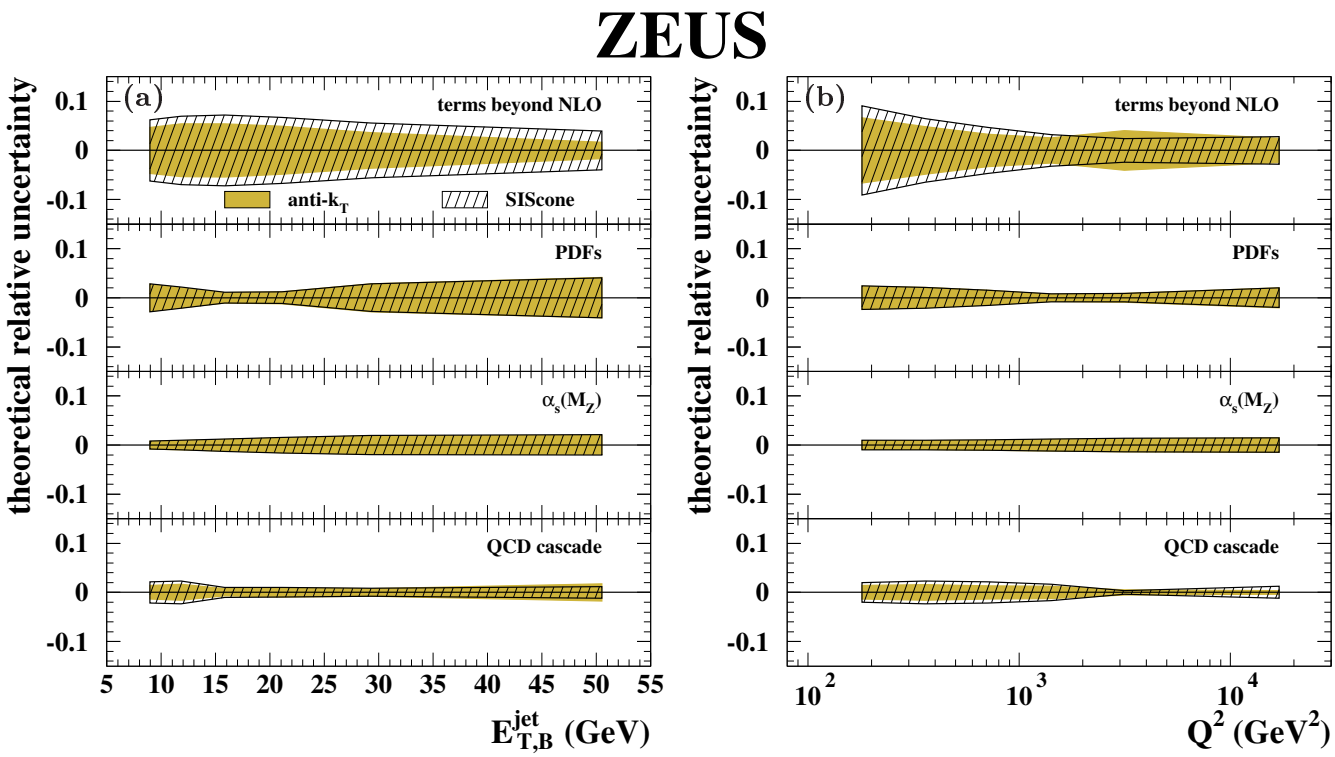

Figure 4: *Overview of the theoretical relative uncertainties for the inclusive-jet cross sections in the kinematic range of the measurements as functions of (a) $E_{T,\mathrm{B}}^{\mathrm{jet}}$ and (b) Q^2 for the anti-k_T (shaded areas) and SIScone (hatched areas) jet algorithms. Shown are the relative uncertainties induced by the terms beyond NLO, those on the proton PDFs, that on the value of $\alpha_s(M_Z)$ and that on the modelling of the QCD cascade.*

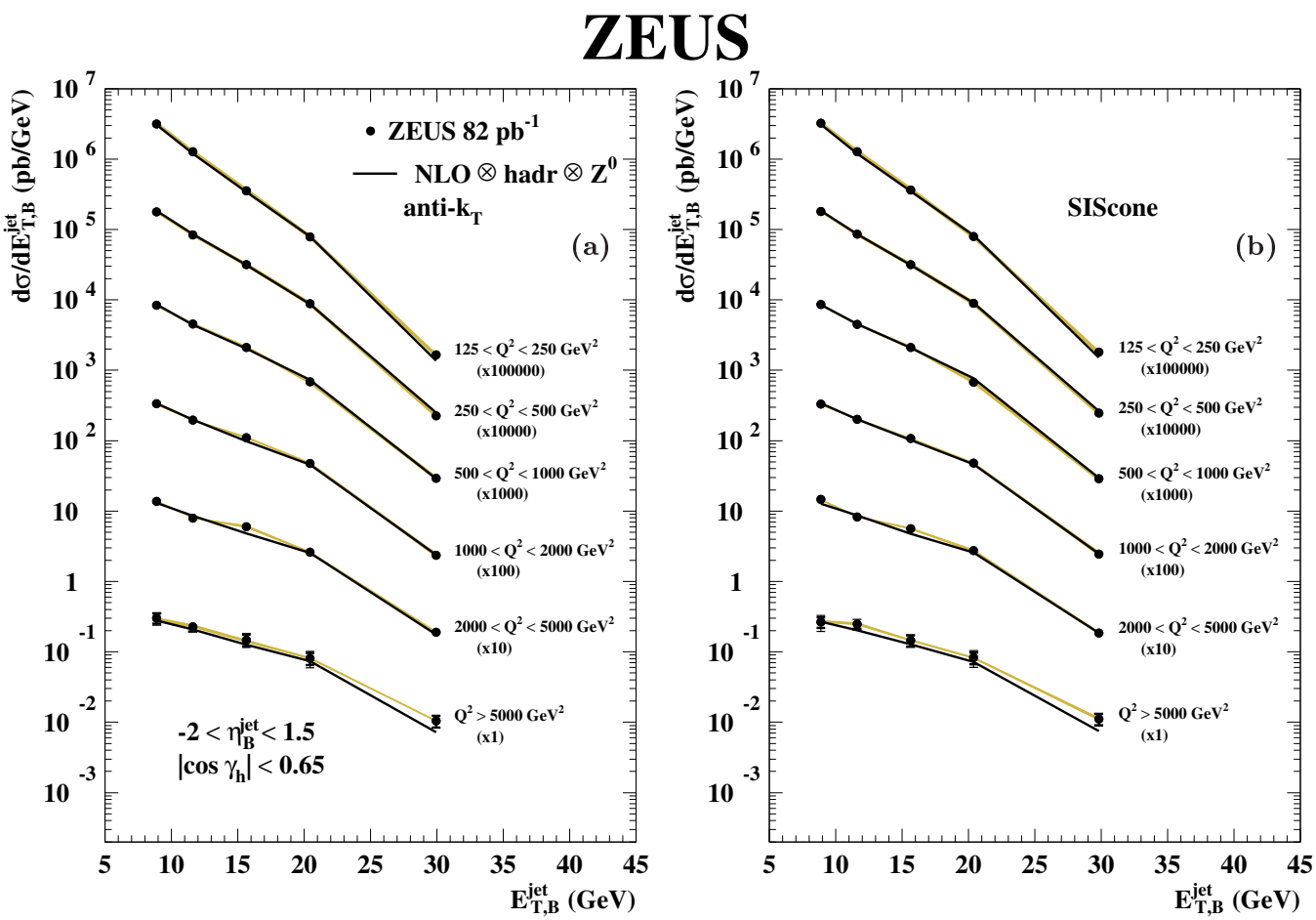

Figure 5: *The measured differential cross-section $d\sigma/dE^{\rm jet}_{T,{\rm B}}$ for inclusive-jet production in different regions of Q^2 (dots) using the (a) anti-k_T and (b) SIScone jet algorithms. The measured and predicted cross sections have been multiplied by a scale factor as indicated in brackets to aid visibility. Other details as in the captions to Figs. 2 and 3.*

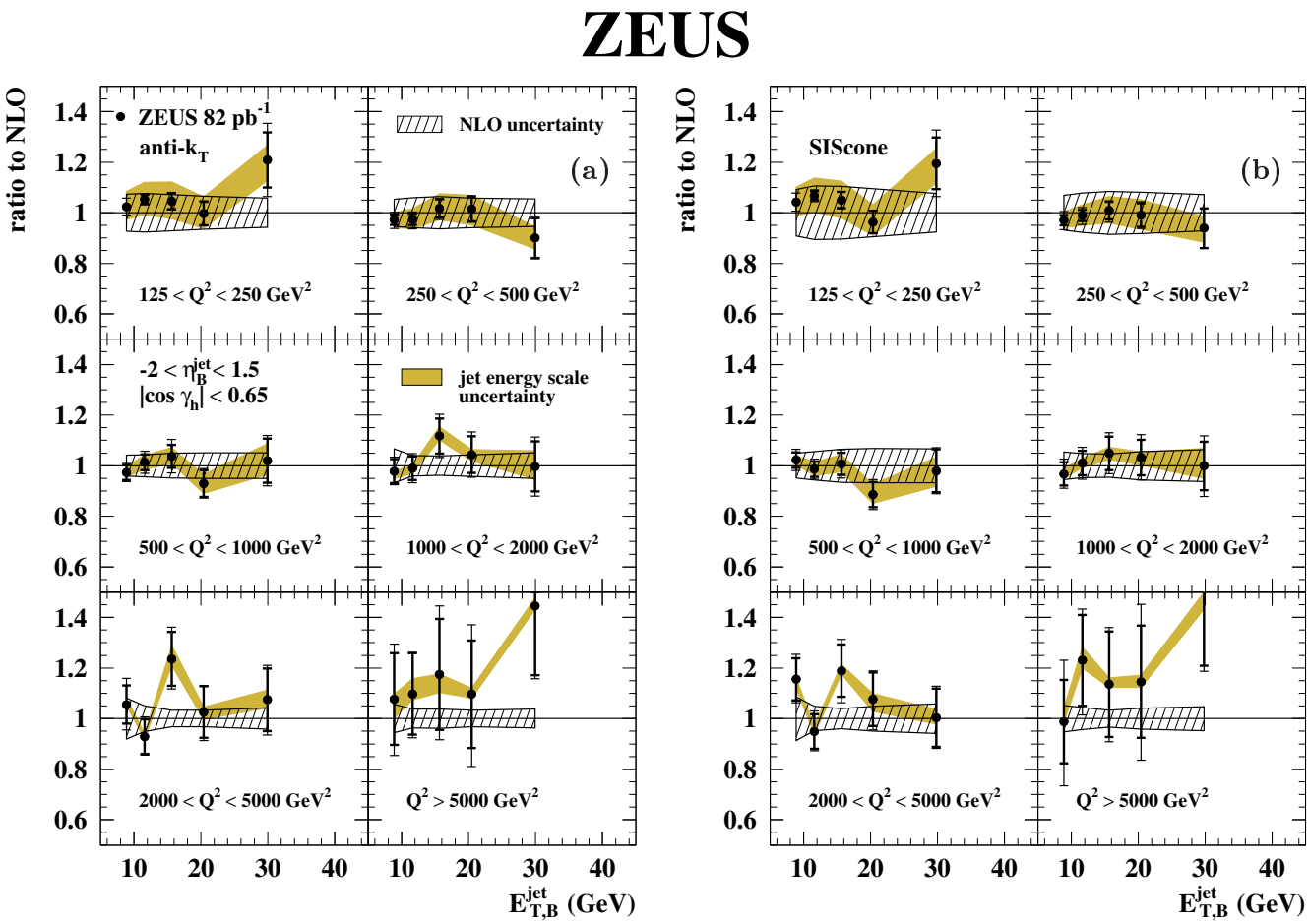

Figure 6: *The ratios between the measured differential cross-sections* $d\sigma/dE^{\rm jet}_{T,\rm B}$ *presented in Fig. 5 and the NLO QCD calculations (dots). Other details as in the captions to Figs. 2 and 3.*